Available online at www.sciencedirect.com
SCIENCE DIRECT®
Journal of Nuclear Materials 351 (2006) 65–77
journal of nuclear materials
www.elsevier.com/locate/jnucmat

Effect of the interatomic potential on the features of displacement cascades in α-Fe: A molecular dynamics study

D. Terentyev [a,b], C. Lagerstedt [c], P. Olsson [d], K. Nordlund [e], J. Wallenius [c], C.S. Becquart [f], L. Malerba [a,*]

[a] SCK•CEN, The Belgian Nuclear Research Centre, Boeretang 200, B-2400 Mol, Belgium
[b] Physique des Solides Irradiés et des Nanostructure CP234s, Université Libre de Bruxelles, Bd. du Triomphe, B-1050 Brussels, Belgium
[c] Department of Nuclear and Reactor Physics, Royal Institute of Technology, Roslagstullsbacken 21, SE-106 91 Stockholm, Sweden
[d] Department of Neutron Research, Ångstrom Laboratory, Uppsala University, Box 525, SE-751 20 Uppsala, Sweden
[e] Accelerator Laboratory, University of Helsinki, POB 43 (Pietari Kalmin katu 2) FIN-00014, Finland
[f] Laboratoire de Métallurgie Physique et Génie des Matériaux, UMR-8517, Université de Lille I, F-59655 Villeneuve d'Ascq cedex, France

Abstract

The primary state of damage obtained in molecular dynamics (MD) simulations of displacement cascades in α-Fe, particularly the fraction of point-defects in clusters, depends on the interatomic potential used to describe the atomic interactions. The differences may influence the microstructural evolution predicted in damage accumulation models which use results from MD cascade simulations as input. In this work, a number of displacement cascades of energy ranging from 5 to 40 keV have been simulated using the same procedure with four different interatomic potentials for α-Fe, each of them providing, among other things, varying descriptions of self-interstitial atoms (SIA) in this metal. The behaviour of the cascades at their different phases and the final surviving defect population have been studied and compared applying the same cascade analysis criteria for all potentials. The outcome is discussed trying to identify the characteristics of the potential that have the largest influence on the predicted primary state of damage.

PACS: 31.15.Qg; 61.72Cc; 34.20Cf; 61.82.Bg

1. Introduction

Displacement cascades are the fundamental process of radiation damage production under neutron and ion irradiation. Their study by means of numerical simulation based on the use of an interatomic potential dates back to the 1960s [1–3]. In these pioneering works, the choice of the potential and the dependence of the results on it were priority issues [1]. On the contrary, over the last 15 years, in spite of a real boom of displacement cascade simulations using many-body potentials [4–17], relatively little attention has been paid to this problem [15,16]. Nonetheless, different potentials do appear to produce cascades with different features, as demonstrated in a review of existing results for α-Fe,

* Corresponding author. Tel.: +32 14 333090; fax: +32 14 321216.
E-mail address: lmalerba@sckcen.be (L. Malerba).

0022-3115/$ - see front matter © 2006 Elsevier B.V. All rights reserved.
doi:10.1016/j.jnucmat.2006.02.020

proposed in these proceedings as companion paper to the present work [17]. Therefore, the question of determining which characteristics of the interatomic potential are mostly responsible for the result of the simulation arises as an important one. This paper strives to address this question, by comparing the characteristics of cascades simulated by molecular dynamics (MD) using four recent potentials for α-Fe, each providing different descriptions of point-defects and featuring different threshold displacement energies (TDE) and stiffness. The comparison is significant because a sufficient number of cascades per case was simulated with the different potentials following exactly the same procedure and analysed using the same criteria. Therefore, differences in the results can only be ascribed to the inherent features of the potential used.

2. Simulation technique

2.1. Interatomic potentials

Four potentials for α-Fe were used for the MD simulations here reported, namely: (i) the short-range (cutoff between 2nd and 3rd nearest neighbour distance) Finnis–Sinclair-type potential proposed by Ackland et al. [18], henceforth denoted as ABC; (ii) the long-range (cutoff between 3rd and 4th nearest neighbour distance) embedded-atom method (EAM) potential fitted by Chakarova et al. [19], henceforth denoted as CWP; (iii) the long-range EAM potential recently developed by Ackland et al. [20], denoted as AMS; and (iv) a version of the long-range EAM potential recently developed by Wallenius et al. [21], denoted as WOL. These potentials were selected for being relatively recent and for providing significantly different descriptions of, in particular, self-interstitial atoms (SIA). While CWP incorrectly predicts the ⟨1 1 1⟩ crowdion to be the most stable configuration, ABC, AMS and WOL feature the correct stability of the ⟨1 1 0⟩ dumbbell. However, the energy difference between these two configurations is very small according to ABC and increasingly larger according to WOL and AMS (see Table 1, where the main properties of the four potentials are summarised). AMS belongs to a family of potentials for α-Fe which has been shown to reproduce fairly closely the behaviour of the SIA as described by ab initio calculations [41]. WOL, on the other hand, predicts formation energies that are too large for all SIA configurations. These different descriptions of the SIA are expected to influence the mobility of SIA and SIA clusters predicted by each of these potentials [42,43]. In particular, the mobility of the SIA will be lower according to AMS, because rotation to and glide along the ⟨1 1 1⟩ direction are not favoured compared to other potentials [43]. The selected potentials also exhibit partially different TDE and different range (R) and stiffness (S). The latter parameters are defined, respectively, as the interatomic distance where the interaction energy equals 30 eV and the gradient of the potential at the same distance. These magnitudes have been introduced in Ref. [44] to describe the behaviour of the potential in the intermediate interval of interatomic distances, where the transition between near-equilibrium atomic oscillations and high-energy regime occurs. In this interval, the many-body potentials used for MD simulations of cascades are typically joined to a high-energy pair potential, more appropriate to describe collisions at close distances (stiffening of the potential, see e.g. [5,8,15]). The most frequently used high-energy pair potential is the so-called ZBL universal potential [45]. The function used to smoothly join the equilibrium potential to the ZBL is *arbitrarily* chosen and the only criterion generally used to test it is that the TDE should be reasonable [5,8,15]. As an illustration of this point, in Fig. 1 the curves for the Fe–Fe pair interaction corresponding to the four potentials used in this work are presented. It can be seen that, although eventually, for high enough energies, all curves join the ZBL, the way the connection is made can greatly differ in the intermediate energy and distance region, thereby leading to possible differences in the cascade outcome. In particular, the parameters R and S have been shown, in a binary collision approximation (BCA) study [44], to correlate with the number of replacement collision sequences (RCS) of the cascade. In addition, the stiffness at higher energies (∼200 eV), here denoted as U, has been seen to influence the cascade density [44]. This BCA study suggests therefore that the features of the function chosen to stiffen the potential may have an important role on the outcome of the cascade. This suggestion is considered and tested here in the case of MD cascade simulations.

2.2. Cascade simulation

All simulations were performed using the MD code Dymoka [15] and following standard practice

Table 1
Summary of the main properties of the four interatomic potentials used in this work for cascade simulations

	ABC	CWP	AMS	WOL	Exp.	Ab initio
Equilibrium properties						
a_0 (Å) (0 K)	2.867	2.866	2.855	2.860	2.86[a]	2.85–2.86[b]
E_{coh} (eV)	−4.316	−4.28	−4.013	−4.28	−4.28[c]	
$\Delta E_{fcc-bcc}$ (meV)	54	50	121	47	50[d]	35[e]
Point-defect energies (eV)						
E_V^f	1.70	1.54	1.71	2.08	2.0 ± 0.2[f], 1.5[g], 1.6 ± 0.10[h], ~1.6–1.75[i]	1.93–2.09[b]
E_V^m	0.78	0.73	0.63	0.81	0.55[j], 0.57 ± 0.14[k]; (1.3) [l,r]	0.59–0.67[b]
$Q^{SD} = E_{V+}^f E_V^m$	2.48	2.27	2.34	2.89	2.48[m]–3.13[n,s]	*2.52–2.76*[b]
$E^f_{\langle 110\rangle}$	4.87	4.15	3.59	6.45	Stable config is $\langle 110\rangle$ db; $E^f = 4.7$–5[o]	3.64[b]
$E^f_{\langle 111\rangle}$	5.00	4.02	4.03	6.87		4.34[b]
$\Delta E_{\langle 111\rangle-\langle 110\rangle}$	0.13	−0.13	0.494	0.42		0.70[b]
TDE (eV)						
$\langle 100\rangle$	18	20	18	22	17[p]	
$\langle 110\rangle$	32	48	34	28	>30[p]	
$\langle 111\rangle$	36	30	34	32	20[p]	
Mean (median)	45.8 ± 0.4 (42)	54.5 ± 0.5 (54)	40 ± 0.3 (36)	41.8 ± 0.3 (38)	(40)[q] (recomm. value)	
Stiffness						
R (Å)	1.18	1.14	1.24	1.03		
S (eV/Å)	−142	−132	−128	−132		
S/R (eV/Å^2)	120	115	103	128		
U (eV/Å)	−852	−879	−852	−1287		

a_0 (lattice parameter); E_{coh} (cohesive energy); $\Delta E_{fcc-bcc}$ (energy difference between the two phases); E_V^f and E_V^m (vacancy formation and migration energy); Q^{SD} (self-diffusion activation energy); $E^f_{\langle 110\rangle}$ and $E^f_{\langle 111\rangle}$ (SIA configuration formation energy); $\Delta E_{\langle 111\rangle-\langle 110\rangle}$ (relative stability of SIA configurations); db (dumbbell); TDE along the three main directions and in average, including median value, see Ref. [22]; S and U (stiffness) and R (range), see text.

[a] Ref. [23].
[b] Ref. [24], unless otherwise specified .
[c] Ref. [25].
[d] Ref. [26].
[e] Ref. [27].
[f] Ref. [28].
[g] Ref. [29].
[h] Ref. [30].
[i] Ref. [31].
[j] Ref. [32].
[k] Ref. [33].
[l] Ref. [34].
[m] Ref. [35].
[n] Ref. [36].
[o] Ref. [37].
[p] Ref. [38].
[q] Ref. [39,40].
[r] The value 1.3 seems to be the result of not high enough purity of Fe [33].
[s] About 15 experimental measurements reported, giving values within this range, see e.g. website: http://diffusion.nims.go.jp/index_eng.html.

[4–16]. A block of atoms was initially equilibrated for 1 ps at 100 K. After equilibration, temperature was not controlled any more (microcanonical statistical ensemble with periodic boundary conditions) as this parameter has been shown to have negligible effect on the cascade simulation results [12,46]. However, the average temperature of the box at the end of the simulation was recorded and was seen never to rise by more than 100–200 K, compared to the initial temperature. The cascade was initiated by imparting the desired kinetic energy to a primary knock-on atom (PKA, or recoil), here referred to as *cascade energy*. Note that this energy will entirely go into defect creation and atomic oscillations, since electronic excitation is not an effect included in the simulation. Therefore, the energy of the corresponding *real*

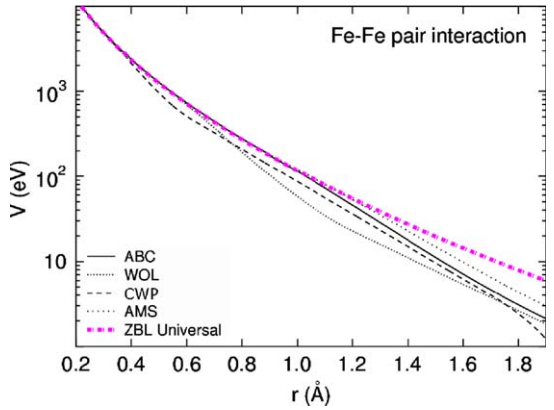

Fig. 1. Fe–Fe pair interaction curves in the energy and distance intermediate region for the four potentials used in this work.

PKA is higher (see e.g. Ref. [12] for a discussion of this point). The PKA was chosen to be at the centre of the cubic box and to move along ⟨1 3 5⟩ directions in order to avoid channelling [11,12]. The cascade energies ranged between 5 and 40 keV and at least 10 cascades per potential and energy were produced. This is on the order of the number of cascade simulations per case typically produced in past, high-energy MD cascade investigations in α-Fe [4–15,46] and is therefore considered to be enough to have statistics comparable with previously published studies. The cascade evolution was visually monitored in each case during the collisional and post-collisional stages, to make sure that there was no self-interaction when boundary crossing occurred [12]. The size of the box was increased for increasing cascade energies, as summarised in Table 2, and the box size/cascade-energy ratio was kept comparable with, or larger than, the same ratio in Ref. [12]. It was decided that the same box size was to be used for simulations of the same

Table 2
Summary of recoil energies, simulation box size and number of simulated cascades in this work

PKA energy (keV)	Box size (number of atoms)	Number of cascades (per potential)
5	250000 ($50a_0$)	10
10	250000 ($50a_0$)	10
15	432000 ($60a_0$)	10
20	432000 ($60a_0$)	10
30	778034 ($73a_0$)	10
40	778034 ($73a_0$)	10[a]

[a] In the case of WOL no 40 keV cascades could be simulated (see text).

Table 3
Time-step scheme used for cascade simulations in this work

Cascade phase	Duration (ps)	Adopted time-step (fs)
Ballistic	0–0.5	0.01
Post-collisional	0.5–3.0	0.05
Recombination	3.0–13.0	0.1
Short-term defect evolution	13.0–23.0	0.5

cascade energy for all four potentials, independently of the cascade volume provided by the potential. This decision made it impossible to simulate 40 keV cascades with WOL, because of the particularly large volume of cascades according to this potential (see below) and the subsequently unavoidable interaction of the cascade with itself through periodic boundary conditions.

In order to ensure that the finite difference method used in the MD code to integrate the equations of motion does not produce uncontrolled errors, the time-step, Δt, was adapted to the cascade phase as summarised in Table 3. During the ballistic phase, when some atoms possess very high kinetic energy and undergo long displacements in very short times, Δt was set to $\sim 10^{-17}$ s (within this time, even the displacement of an Fe atom with 40 keV of kinetic energy is still on the order of 10^{-3} nm, which is sufficiently short to guarantee the stability of the algorithm). During the post-collisional phase, in order to speed up the simulation without affecting the precision, Δt was extended to $\sim 10^{-16}$ s. After the recombination phase of the cascade, the near-equilibrium evolution was followed for $\sim$23 ps using, for the last 10 ps, the typical time-step of MD simulations ($\Delta t \sim 10^{-15}$ s), until the block of atoms was fully thermalised. The temperature reached in the box at this point was recorded and used to determine the temperature increase induced by the introduction of the PKA.

2.3. Cascade analysis

Point-defects were identified and counted in two ways: (1) using the Wigner–Seitz (WS) cell method, and (2) using 'displacement' (also called 'equivalent spheres') analysis. The former method requires WS cells to be defined around each perfect lattice position: an empty cell means a vacancy, while two (or more) atoms in the same cell mean an interstitial configuration. The second method corresponds to using spheres instead of WS cells: the distance

between the perfect lattice position and the displaced atom is measured and appropriate cutoff radii are used to decide whether a displacement has occurred and to identify the defect type [5,8]. This method was mainly used for comparison purposes, to make sure that the criterion used to identify point-defects did not significantly influence the results of the analyses. Either way, the evolution in time of the number of defects can be monitored so as to identify (i) the peak stage, in terms of time since cascade initiation, in correspondence with the maximum number of defects, (ii) the recombination, or relaxation, phase and (iii) the number of surviving Frenkel pairs (FP). The defect analysis also allowed the defect positions to be recorded, thereby enabling the cascade evolution to be visualised with the aid of appropriate tools. Through visualisation, a rough estimate of the number of subcascades produced at high enough energy could be given as well.

As an indication of the duration of the recombination phase, which is roughly coincident with the thermal spike, the characteristic relaxation time, τ_r, was also determined. Following Calder and Bacon [5], this parameter was estimated using an exponential decay approximation from peak time (t_{peak}) for the number of FP (v_{FP}) as a function of time: $\{v_{FP} - v_{FP}^{end}\}(t - t_{peak}) = A\exp[-(t - t_{peak})/\tau_r]$, where v_{FP}^{end} is the number of FP that survived recombination at the final, steady state of the cascade.

The cascade volume and density at peak stage were evaluated using so-called *component analysis*, described in detail elsewhere [47,48]. According to this procedure, the volume of the cascade is associated with an ellipsoid, whose axes (*components*) are defined based on the variance of the spatial point-defect distribution. The major axis has the direction maximising the variance, the second one maximises the variance of the distribution projected onto a plane perpendicular to the first one, and the third one has the direction minimising this variance. These directions are parallel to the directions of the eigenvectors of the covariance matrix of the point-defect distributions and the associated eigenvalues are the variances of the distribution projected onto the directions of the eigenvectors. Thus, the problem is reduced to the diagonalisation of a 3×3 symmetrical, real and positive matrix, which is a straightforward operation. This method is of course not completely justified when subcascade formation becomes important. Still, it provides a reference for comparison purposes, if used systematically for all cascades.

The number of defects in clusters (and the number of clusters) produced during the evolution of the cascade were determined using an automated procedure: point-defects located at a mutual distance below a certain cutoff were searched for and associated with the same cluster. However, the situation at the end of the cascade was further analysed by visual inspection. Different criteria (i.e. different cutoff distances) for the automated procedure were used: vacancy clusters were defined using both 2nd and 4th nearest neighbour (nn) criteria [12] and SIA clusters using both 1st [8,15] and 3rd nn [49] criteria. The visual inspection was used in addition because it has been observed that automated procedures tend to provide somewhat smaller fractions of SIA in clusters [50].

3. Results

3.1. Peak stage and recombination phase

The main features characterising the cascade peak stage are the maximum number of defects, the time elapsed from the initiation of the cascade when this number is reached (peak time), the cascade volume (according to the component analysis) and the cascade density (i.e. the number of defects per unit volume, given by the ratio between the maximum number of defects and the cascade volume, as provided by the component analysis), all of them as functions of cascade energy. Another feature that can be roughly estimated by visually inspecting the shape of the cascade at peak time is the number of subcascades.

The number of defects and the cascade density at peak time are shown in Fig. 2 for all four potentials used in this work. Clearly, WOL provides significantly less defects at peak time than any other potential and the cascade density is the smallest as a consequence of a large average cascade volume (figure not shown). At the other extreme, AMS produces the largest number of defects at peak time (a factor 2–5 compared to WOL) and exhibits the highest cascade density. The other two potentials lie in-between, with the ABC density closer to AMS and the CWP density closer to WOL. Fig. 3 shows the relaxation time as a function of cascade energy for the four potentials and it appears that the potential ranking according to this parameter is roughly the same as for the peak number of defects and cascade density. This fact will be discussed below.

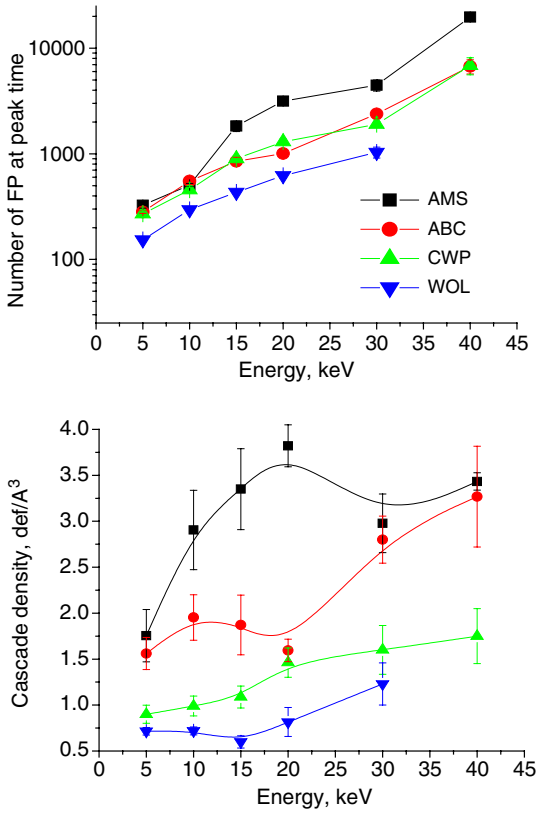

Fig. 2. Number of defects (above) and cascade density (below) at peak time versus cascade energy according to the four potentials used in this work. Lines are guides for the eyes. Note that the error bars in the number of defects are 'smaller than the symbol'.

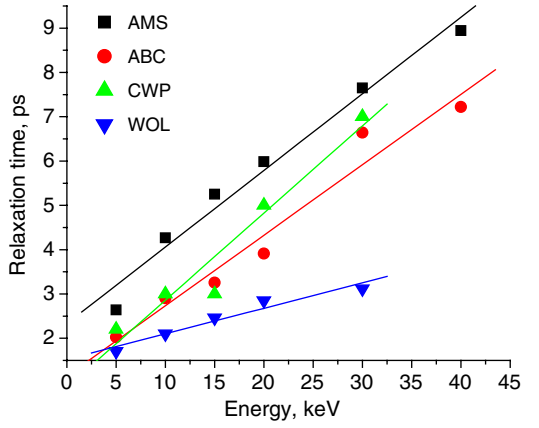

Fig. 3. Relaxation time versus cascade energy according to the four potentials used in this work. Lines are linear interpolations used as guides for the eyes.

Fig. 4 shows the average number of subcascades produced versus cascade energy, obtained by visual

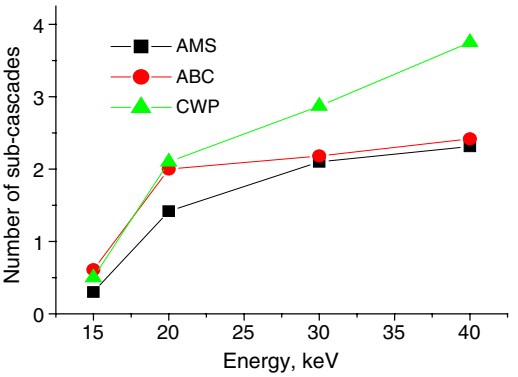

Fig. 4. Estimated average number of subcascades (in addition to the single cascade always produced) versus cascade energy according to the four potentials used in this work, after visual inspection. Lines are guides for the eyes. The estimation is necessarily only a very rough one.

inspection. With WOL, the cascades appeared too dilute for subcascades to be identified, so no curve is given. These curves must be taken as indicative only, due to the arbitrariness of the criterion used to define a subcascade (visual appearance) and to the fact that the number of simulated cascades is too small to consider the sample statistically representative and to be fully quantitative in this particular case. The impression is, however, that only above 20 keV can the average number of subcascades be larger than one, i.e. cascade splitting actually occurs only above this threshold, in agreement with what was reported by Stoller [12]. Finally, CWP seems to exhibit a stronger tendency to result in cascade splitting than the other potentials.

3.2. Primary state of damage

3.2.1. Defect production efficiency

Fig. 5 presents the defect production efficiency, $\eta = \nu_{FP}^{end}/\nu_{NRT}$, versus cascade energy, for all four potentials considered in this work. Here, $\nu_{NRT} = 0.8E_D/2E_d$ is the standard number of NRT displacements [51], where E_D is the damage energy, coincident with the cascade energy in the MD simulation (i.e. the kinetic energy imparted to the recoil in the simulation), and E_d is an average TDE which, following common practice [7,12,15,39,40,52], has been taken to equal 40 eV. Potentials providing different TDE (Table 1), as well as different numbers of defects and densities at peak time (Fig. 2), produce roughly the same number of defects at the end of the simulation. The only partial exception is WOL, which stands out for a slightly higher η

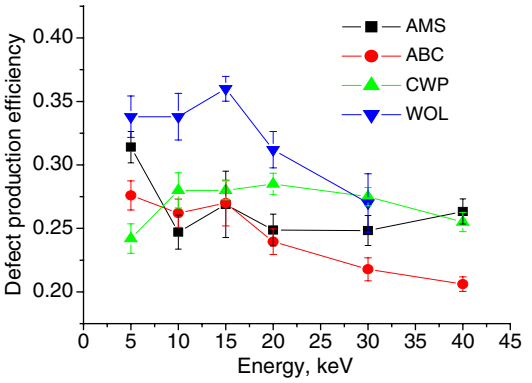

Fig. 5. Defect production efficiency compared to NRT displacements (see text) according to the four potentials used in this work.

(note that at peak time this potential produced the *fewest* defects). However, all potentials agree in providing efficiencies in the 0.3 ± 0.1 range, in line with results obtained with other potentials available from the literature and in agreement with existing experimental assessments (see Ref. [17] for a discussion on this point). AMS seems to exhibit a minimum efficiency at 10 and 20 keV, the latter minimum being in agreement with the behaviour observed by Stoller and attributed to onset of cascade splitting [12]. However, CWP displays a minimum at 5 keV which is not ascribable to subcascade formation above this energy (Fig. 4) and ABC presents an η steadily decreasing with increasing cascade energy, so most likely these minima and maxima should be attributed to statistic fluctuations. The main observation is that no significant difference is found in the amount of surviving FP going from one potential to another at the same cascade energy.

3.2.2. Defect clustered fractions

The fraction of point-defects found in clusters and the cluster size distribution are fundamental information provided by displacement cascade studies to be used as input in damage accumulation models [53]. In Fig. 6, the point-defect clustered fraction, f_t^{cl} ($t =$ V or SIA), is given as a function of cascade energy for the four potentials: $f_{\mathrm{SIA}}^{\mathrm{cl}}$ was determined by visual inspection, while $f_{\mathrm{V}}^{\mathrm{cl}}$ is the result of an automated analysis using a 2nd nn criterion. These magnitudes are known to be affected by large oscillations and a completely smooth, monotonous behaviour versus cascade energy is hardly ever obtained [12,15]. However, trends can be identified.

In broad agreement with observations made in previous works [7,9,12–14], the SIA clustered fraction tends to increase with increasing cascade energy until saturation well into the subcascade regime. This increase is particularly steep according to CWP and much less according to the other potentials. This fact may have some relationship with the tendency of CWP to form more subcascades (Fig. 4) since subcascade overlap seems to favour the formation of larger clusters [50]. AMS tends to produce smaller fractions of SIA in clusters than the others.

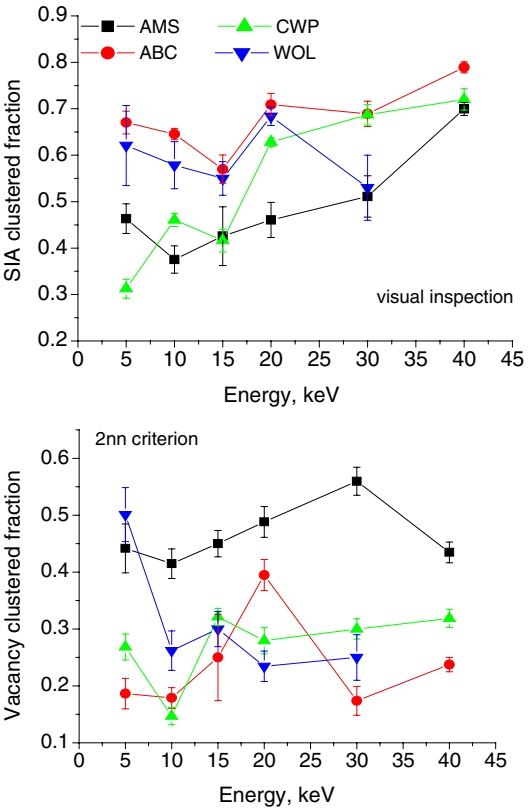

Fig. 6. Fraction of SIA (above) and vacancies (below) in cluster according to the four potentials used in this work. The SIA clustered fraction was determined by visual inspection, while for the vacancies an automated procedure with 2nd nn distance criterion was applied.

The vacancy clustered fraction, with the exception of a few outlying points, remains fairly constant for all potentials at all cascade energies. Its value is around 0.2–0.3 for three of the four potentials, but AMS stands out for a particularly high value ($f_{\mathrm{V}}^{\mathrm{cl}} \sim 0.4$–$0.5$). This value broadly equals the fraction of SIA in clusters produced by the same potential, which therefore predicts the same amount of vacancies and SIA in cluster.

4. Discussion

4.1. Number of surviving defects

It is perhaps surprising that potentials which: (i) give different descriptions of point-defects, (ii) predict different TDE and (iii) provide largely different numbers of defects and cascade densities at peak time, end up producing essentially the same number of surviving FP. There must be features of the potentials that induce opposite effects, which compensate each other. As explained in what follows, Figs. 2 and 3 suggest that the mutually offsetting results may be higher cascade density (and number of defects) at peak time, followed by longer relaxation (recombination) times.

As anticipated in the introduction, work on comparison of potentials performed in the BCA has shown that the stiffness S and the range R at 30 eV correlate with the production of RCS: stiffer and shorter-ranged potentials (i.e. characterised by a high S/R ratio) favour the process of energy transfer during the binary collision, thereby favouring the production of more, and longer, RCS [44]. Clearly, this mechanism of defect production favours the spreading of the cascade over large volumes and penalises defect recombination. In our study, WOL exhibits the largest S/R ratio (see Table 1) and the cascades produced with this potential have the lowest density and a slightly higher number of surviving defects. In addition, at peak time WOL cascades appear very dilute, suggesting that indeed a significant part of the FP were the consequence of RCS (Fig. 7). This is in contrast with the 'cascade regime', observed and described by Calder and Bacon for cascades above 1 keV [5], characterised by shock-induced collective effects whereby whole regions of the crystal are displaced along close-packed directions. This regime seems to be easily reached with the other three potentials and in the case of AMS, which presents the smallest S/R ratio (103), very dense and compact cascades are produced (Fig. 7). In line with these observations, it has been observed in Ref. [17] that the potential there denoted as HA-VD [8] has the highest S/R ratio of all (146) and that indeed this potential produces very dilute cascades, with an abnormally high number of surviving FP, as reported also in Ref. [15]. Thus, it appears that the correlations observed in the BCA study of Ref. [44] between potential stiffness and cascade density or number of RCS hold also in MD simulations, although in our simulations the role of the stiffness U at 200 eV does not appear to be significant. Too high a stiffness and, more importantly, too short a range in the ~30 eV energy region, hinders the attainment of a full cascade regime. On the contrary, the attainment of the cascade regime is favoured when the potential is soft and long-ranged in the ~30 eV energy region.

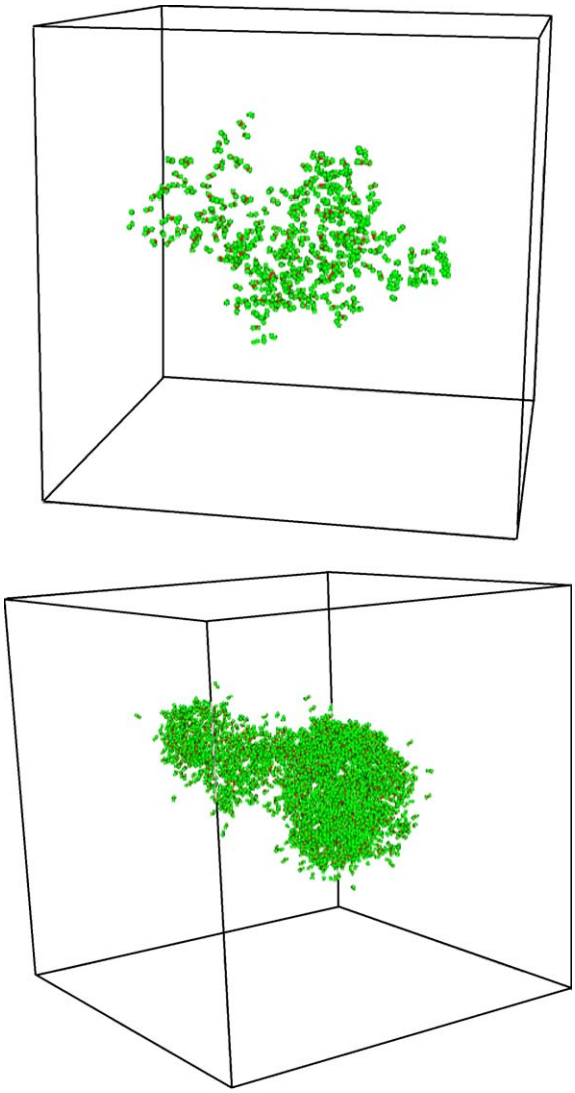

Fig. 7. Appearance at peak time of a typical 20 keV cascade simulated with WOL (above) and with AMS (below). The two potentials predict opposite cascade behaviour and the former is the softest, while the latter is the stiffest (at ~200 eV).

A full cascade regime involves a high-energy density at peak time and the production of a state close to a melt [5]: how close will depend on the actual defect density at peak time and also on the melting

point predicted by the potential. The cascade density is therefore an index of the attainment of the cascade regime. In addition, in a dense and partially melted cascade region, the thermal spike will last longer and lead to more recombinations than in a dilute and still solid cascade region, where defects have been produced mostly by RCS. Consistently, Figs. 2 and 3 show that a higher density correlates not only, as is obvious, with a higher number of peak time defects but also, roughly, with a longer relaxation time, i.e. with longer thermal spikes and more defect recombination. If a simplified picture based on the S/R ratio is adopted for the four potentials used in this work, both the density of the cascade and the relaxation time can be said to scale with the reverse of this ratio. The level of the curves in Figs. 2 and 3 can be hence roughly anticipated from the S/R value. Low-S/R potentials, such as AMS, induce a full cascade regime and produce at peak time a much higher number of atomic displacements through collective motion (without RCS). However, in this case recombination will also be more important. The two phenomena (a large number of defects at peak time and a long relaxation time), although having the same origin (low S/R), will therefore offset each other, eventually leading to a similar number of surviving FP as for potentials with higher S/R. On the other hand, high-S/R potentials will exhibit a smaller peak defect number, but also a shorter recombination time and, therefore, a number of surviving defects similar to that of low-S/R potentials.

Nonetheless, high-S/R potentials, such as WOL, can still produce a higher number of surviving defects, because relaxation is not, or only marginally, assisted by thermal effects and the larger dilution of damage reduces the probability of spontaneous recombination between SIA and vacancies. This effect is only mildly visible in WOL but reaches an extreme manifestation in the case of the HA-VD potential [8,15] discussed in Ref. [17].

Thus, potential range and stiffness (R, S and possibly also U) appear to offer a means to rationalise some of the cascade features that vary from one potential to another. On the contrary, however surprising it may seem, no explicit correlation is found between the number of defects, both at peak time and in the final defect state, and the TDE values. The potential with the largest average TDE (CWP) *does not* produce the smallest number of defects, during any of the phases of the cascade.

4.2. Clustered fraction

While the stiffness of the potential seems to be of use to explain the differences concerning defect production, it is not as useful when it comes to rationalise differences in defect clustered fractions. In this case, the potential exhibiting the most peculiar behaviour is AMS, for which it is easy to see (Fig. 6) that the difference $f_{\mathrm{SIA}}^{\mathrm{cl}} - f_{\mathrm{V}}^{\mathrm{cl}}$ is very close to zero in most cases. The other potentials display more uniform behaviour, although the steep increase of $f_{\mathrm{SIA}}^{\mathrm{cl}}$ with CWP stands out as a peculiarity, too. In order to try to understand the reasons for the differences between AMS and the other potentials, the evolution of the clustered fraction for 23 ps after peak time has been monitored using automated procedures for both vacancies (2nd nn criterion) and SIA (3rd nn criterion). An example is given in Fig. 8 for cascades at 15 keV (the results

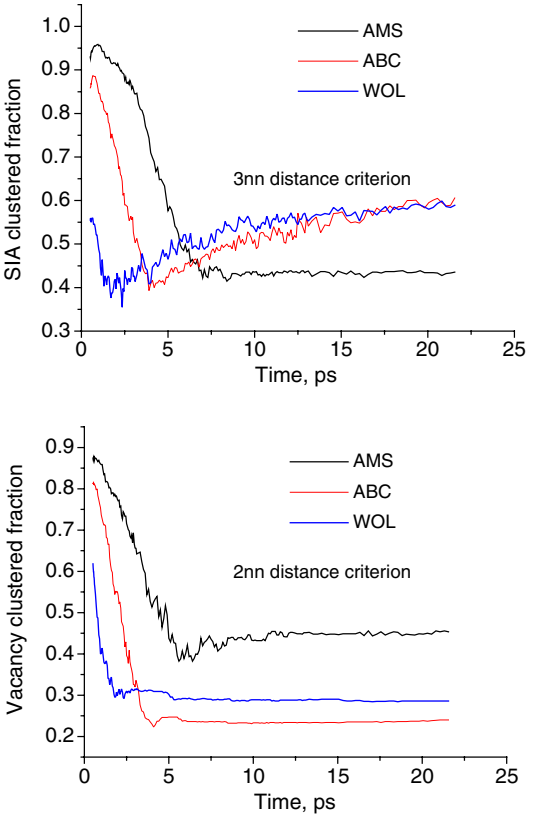

Fig. 8. Evolution in time of the fraction of SIA (above) and vacancies (below) in cluster in 15 keV cascades, according to potentials AMS, ABC and WOL (CWP provides results extremely similar to ABC and the relevant curves are therefore not shown). SIA and V clusters are defined, respectively, using a 3rd nn and a 2nd nn criterion.

for CWP are not presented because they are almost coincident with those of ABC). The reader should be warned that, strictly speaking, clusters cannot be defined at peak time based on a lattice site occupation criterion. In this case, the 'clustered fraction' as we define it is in fact simply an index of how many of the displaced atoms appear to be at a mutual distance comparable to the distance between defects in a cluster or, in the case of vacancies, how many cavities are formed during the cascade evolution. The physical interpretation of the 'clustered fraction' versus time will therefore keep changing, as will be clear in the discussion below.

According to Bacon et al. [9], two mechanisms of SIA cluster in-cascade formation can be devised. Partly they form at the end of the thermal spike, as a consequence of collective atomic motion in conditions of highly enhanced defect diffusion, due to high local temperature; partly by later local defect re-organization, driven by strain-field interaction among neighbouring and mobile SIA and SIA clusters. The upper graph in Fig. 8 reveals that both mechanisms may occur, but their respective weight is different depending on the potential. According to both AMS and ABC, the 'clustered fraction' at peak time is close to unity. Since, as mentioned, speaking of clusters is inappropriate at peak time, this is a way of saying that collective atomic displacements are taking place, whereby the displaced atoms remain all very close to each other (high density) and are therefore recognised 'as if' they were forming clusters. However, during relaxation this 'clustered fraction' drops by about 50%. WOL, on the other hand, produces only a relatively small SIA 'clustered fraction' at peak time, a sign that little or no collective displacement of atoms occurs, in agreement with the above discussion on the dilution of damage, and the subsequent drop is limited to about 10%. That is, with WOL even at peak time the computed 'clustered fraction' is mostly due to actual clusters. After relaxation, when the plotted clustered fraction becomes indeed the result of defect clustering, WOL and ABC exhibit similar behaviour: SIAs rearrange themselves into an increasing fraction of defects in cluster, via (perhaps thermally enhanced) diffusion. On the contrary, the fraction of SIA in clusters remains unchanged according to AMS. This is probably the effect of the different SIA mobility predicted by the two classes of potentials. According to AMS, glide of the SIA along the $\langle 1\,1\,1\rangle$ close-packed direction is unlikely, because of the large difference between the stable $\langle 1\,1\,0\rangle$ configuration and the $\langle 1\,1\,1\rangle$ crowdion configuration (see Table 1), which prevents rotation from one to the other. Migration is therefore fully three-dimensional and relatively slow, with an effective energy of $\sim$0.3 eV [41,43]. On the contrary, according to the other two potentials glide is possible and the effective SIA migration energy is much lower (a few tens of meV) with a consequently higher mobility [42,43]. Thus, SIA re-organization via diffusion is possible on the scale of ps with all potentials, except with AMS.

Concerning vacancies, because of their much slower diffusivity compared to SIA, very similarly described by all potentials (Table 1), clustering is a priori only expected to occur during the ballistic phase and the thermal spike (unless collapse, so unusual in α-Fe, occurs [49]). The lower graph of Fig. 8 shows, however, that this is not always the case. The peak and relaxation time behaviour is, with the three potentials, similar to the SIA case. But later, three different evolutions are possible. According to WOL, the vacancy clustered fraction experiences a mild decrease, most likely because of further, diffusion-driven recombination with rapidly migrating SIA. According to ABC the clustered fraction remains essentially unchanged. But according to AMS a clear increase is seen to occur. This is difficult to explain, because vacancy diffusion should be negligible on a ps scale. Different factors may combine to produce this post-relaxation vacancy clustering. The density of the cascade may be so high that a very small number of vacancy jumps may be sufficient to drive further clustering. Alternatively (or in addition), the temperature in the cascade region during this phase may for AMS be locally closer to the melting point predicted by the potential, thereby allowing enhanced vacancy diffusion and clustering compared to the other potentials. In fcc metals, for example, it has been shown that the melting point affects the ion beam mixing and how vacancies are pushed towards the centre of the cascade to cluster [54]. In particular, the fact that following relaxation AMS exhibits a larger f_V^{cl} compared to the other potentials may be related to partial cascade collapse during the thermal spike and may correlate with either a lower melting point predicted by the potential or a higher cascade core temperature, due to the high density, or both. However, the effect of the melting point becomes negligible when the density of defects is not especially high. Indeed, the melting point of CWP has been calculated to be between 1800 and

1850 K [55], while the melting point of ABC is around 2200 K [56], but no difference in vacancy clustering has been observed. Further studies are therefore in course to clarify the origin of this behaviour of AMS [57]. Still, it is clear that the clustered fractions predicted by a certain potential are determined by a complicated combination of interacting factors, related partly to the point-defect mobility according to the potential, partly to the description that the potential gives of the cascade regime (i.e. to the influence of its stiffness in the repulsive region) and partly to other properties, such as the melting point.

5. Conclusions

The main goal of the present paper, driven by the review done in Ref. [17], was to produce a set of cascade results for different potentials, adopting standard simulation procedures and rigorously identical analysis techniques, in order to find out whether different potentials provide different results and which, among the potential features, are primarily responsible for the differences. It can be concluded that:

- The number of Frenkel pairs produced in a cascade during the whole displacement process *does not* correlate with the threshold displacement energies predicted by the potential (provided that these are reasonable).
- A correlation is found instead with the stiffness and range of the potential in the region of tens of eV interaction, as suggested by BCA studies [44], i.e. in the region of transition between equilibrium and repulsive potential, which is largely arbitrary [5,8,15]. With potentials too stiff and short-ranged in the 30 eV energy region replacement collision sequences become the main mechanism of damage production and a full cascade regime is never reached, even at high cascade energies. The dilute damage produced at peak time in these cases exhibits fewer defects and, on average, a larger distance between SIA and their vacancies (low density), partially preventing SIA-vacancy recombination during relaxation. On the other hand, a full cascade regime, characterised by collective atomic displacements, massive defect production at peak time, higher damage density and a pronounced thermal spike, is typical of potentials which are soft and long-ranged at $\sim$30 eV. The length of the thermal spike in this case may however also be influenced by the melting point predicted by the potential.
- In spite of largely different cascade processes, all potentials predict roughly the same final amount of surviving Frenkel pairs (with the only exception of specially pathological cases, as discussed in Ref. [17]). This is likely to be the result of mutually offsetting effects of the stiffness-to-range ratio. A low ratio ('soft' potentials) causes a higher defect density at peak time, but also induces, as a consequence, a longer relaxation time with more recombinations. A high ratio ('hard' potential) leads to reduced defect production at peak time but also to reduced recombination during relaxation. As a consequence, the final number of surviving defects appears to be largely independent of the cascade features at peak time.
- Vacancy and SIA in-cascade clustering are potential dependent. Differences are the result of a complicated interplay between different features of the potential, from the description of the mobility of point-defects, to the density of the cascade at peak time (related to the stiffness) and the extent of the thermal spike, as well as the possibility of cascade collapse, which may also depend on the melting point predicted by the potential.

The most worrying conclusion is that the result of cascade simulations using a given potential may be greatly influenced by the partially arbitrary choices made when stiffening the potential in the region of tens to hundreds of eV [5,8,15], i.e. in the region of the transition between the equilibrium part of the potential and the high-energy ZBL pair potential typically used for very short interatomic distances [45]. The fit to the TDE in that region appears to be of little use as a guide for the stiffening [17]. For example, would cascades simulated with the AMS potential, probably the best one available right now for radiation damage in α-Fe, still predict the same large amount of vacancies in clusters, if the connection in the transition region was significantly stiffer at tens of eV? For the moment, there is no answer to this question.

Acknowledgements

This work required a fairly large amount of CPU time to be performed: four PC clusters, at

SCK•CEN, KTH, U. Uppsala and ULB (thanks to M. Hou for allowing its use) were simultaneously exploited for the task. This work, supported by the European Commission under the contract of Association between Euratom and the Belgian, Swedish and Finnish States, was carried out within the framework of the European Fusion Development Agreement (EFDA), task TTMS-007.

References

[1] J.B. Gibson, A.N. Goland, M. Milgram, G.H. Vineyard, Phys. Rev. 120 (4) (1960) 1229.
[2] C. Erginsoy, G.H. Vineyard, A. Englert, Phys. Rev. 133 (2A) (1964) A595.
[3] C. Erginsoy, G.H. Vineyard, A. Shimizu, Phys. Rev. 139 (1A) (1965) A118.
[4] C.A. English, A.J.E. Foreman, W.J. Phythian, D.J. Bacon, M.L. Jenkins, Mater. Res. Forum 97–99 (1992) 1.
[5] A.F. Calder, D.J. Bacon, J. Nucl. Mater. 207 (1993) 25.
[6] D.J. Bacon, T. Díaz de la Rubia, J. Nucl. Mater. 216 (1994) 275.
[7] D.J. Bacon, A.F. Calder, F. Gao, V.G. Kapinos, S.J. Wooding, Nucl. Instrum. and Meth. B 102 (1995) 37.
[8] R. Vascon, N.V. Doan, Radiat. Eff. Def. Solids 141 (1997) 375;
N.V. Doan, R. Vascon, Ann. Phys. C3 20 (Suppl. 3) (1995) 57.
[9] D.J. Bacon, A.F. Calder, F. Gao, J. Nucl. Mater. 251 (1997) 1.
[10] R.S. Averback, T. Díaz de la Rubia, Sol. State Phys. 51 (1998) 281.
[11] N. Soneda, T. Díaz de la Rubia, Philos. Mag. A 78 (5) (1998) 995.
[12] R.E. Stoller, J. Nucl. Mater. 276 (2000) 22;
R.E. Stoller, G.R. Odette, B.D. Wirth, J. Nucl. Mater. 251 (1997) 49.
[13] D.J. Bacon, F. Gao, Yu. Osetsky, J. Nucl Mater. 276 (2000) 1.
[14] D.J. Bacon, Yu.N. Osetsky, R.E. Stoller, R.E. Voskoboinikov, J. Nucl. Mater. 323 (2003) 152.
[15] C.S. Becquart, C. Domain, A. Legris, J.-C. van Duysen, J. Nucl. Mater. 280 (2000) 73.
[16] Yu.N. Osetsky, D.J. Bacon, Nucl. Instrum. and Meth. B 180 (2001) 85.
[17] L. Malerba, J. Nucl. Mater., these proceedings, doi:10.1016/j.jnucmat.2006.02.023.
[18] G.J. Ackland, D.J. Bacon, A.F. Calder, T. Harry, Philos. Mag. A 75 (1997) 713.
[19] R. Chakarova, V. Pontikis, J. Wallenius, Development of Fe(bcc)–Cr many body potential and cohesion model, Delivery report WP6, SPIRE project, EC contract no. FIKW-CT-2000-00058, June 2002. Available from: <www.neutron.kth.se/publications/library/DR-6.pdf>;
P. Olsson, L. Malerba, A. Almazouzi, SCK•CEN Report, BLG-950, June 2003.
[20] G.J. Ackland, M.I. Mendelev, D.J. Srlolovitz, S. Han, A.V. Barashev, J. Phys.: Condens. Matter 16 (2004) 1.
[21] J. Wallenius, P. Olsson, C. Lagerstedt, Nucl. Instrum. and Meth. B 228 (2005) 122.
[22] K. Nordlund, J. Wallenius, L. Malerba, Nucl. Instrum. and Meth. B, submitted for publication.
[23] G. Simmons, H. Wang, Single Crystal Elastic Constants and Calculated Aggregate Properties: A Handbook, MIT, Cambridge, 1971.
[24] C. Domain, C.S. Becquart, Phys. Rev. B 65 (2001) 024103; C.-C. Fu, F. Willaime, P. Ordejón, Phys. Rev. Lett. 92 (17) (2004) 175503.
[25] C. Kittel, Introduction to Solid State Physics, 6th Ed., John Wiley, 1987.
[26] W. Bendick, W. Pepperhof, Acta Metall. 30 (1982) 679.
[27] E.G. Moroni, G. Kresse, J. Hafner, J. Furthmüller, Phys. Rev. B 56 (1997) 15629.
[28] L. De Schepper et al., Phys. Rev. B 27 (9) (1983) 5257.
[29] K. Maier, H. Metz, D. Herlach, H.-E. Schaefer, J. Nucl. Mater. 69&70 (1978) 589.
[30] H.-E. Schaefer et al., Scr. Metall. 11 (1977) 803;
H. Matter, J. Winter, W. Triftshäuser, Appl. Phys. 20 (1979) 135.
[31] K. Fürderer et al., Mater. Sci. Forum 15–18 (1987) 125;
A. Seeger, Phys. Stat. Sol. (a) 167 (1998) 289.
[32] L.J. Cuddy, Acta Metall. 16 (1968) 23.
[33] T. Tabata et al., Scr. Metall. 14 (1983) 1317.
[34] C.H. Woo, W. Frank, Radiat. Eff. 77 (1983) 49;
F. Philipp, Mater. Sci. Forum 15–18 (1987) 187.
[35] F.S. Buffington, K. Hirano, M. Cohen, Acta Metall. 9 (1961) 434.
[36] V.M. Amonenko, A.M. Blinkin, I.G. Ivantsov, Phys. Met. Metall. 17 (1) (1964) 54.
[37] H. Wollenberger, in: R. Cahn, P. Haasen (Eds.), Physical Metallurgy, vol. 2, North-Holland, 1996.
[38] F. Maury, M. Biget, P. Vajda, A. Lucasson, P. Lucasson, Phys. Rev. B 14 (1976) 5303.
[39] Annual Book of ASTM Standard E693-94, vol. 12.02, 1994.
[40] C.H.M. Broeders, A.Yu. Konobeyev, J. Nucl. Mater. 328 (2004) 197.
[41] F. Willaime, C.-C. Fu, M.C. Marinica, J. Dalla Torre, Nucl. Instrum. and Meth. B 228 (2005) 92.
[42] Yu.N. Osetsky et al., J. Nucl. Mater. 276 (2000) 65.
[43] D. Terentyev, L. Malerba, M. Hou, Mobility of self-interstitial atom clusters in N1–Fe: a "new" molecular dynamics study, submitted for publication.
[44] C.S. Becquart, A. Souidi, M. Hou, Phys. Rev. B 66 (2002) 134104.
[45] J.F. Ziegler, J.P. Biersack, U. Littmark, The Stopping and Range of Ions in Matter, Pergamon, New York, 1985.
[46] F. Gao, D.J. Bacon, P.E.J. Flewitt, T.A. Lewis, J. Nucl. Mater. 249 (1997) 77.
[47] M. Hou, Phys. Rev. B 31 (7) (1985) 4178.
[48] A. Souidi, M. Hou, C.S. Becquart, C. Domain, J. Nucl. Mater. 295 (2001) 179.
[49] N. Soneda, S. Ishino, T. Díaz de la Rubia, Philos. Mag. Lett. 81 (9) (2001) 649.
[50] D.A. Terentyev, L. Malerba, M. Hou, Nucl. Instrum. and Meth. B 228 (2005) 156.
[51] M.J. Norgett, M.T. Robinson, I.M. Torrens, Nucl. Eng. Des. 33 (1975) 50.
[52] W.J. Phytian, A.J.E. Foreman, R.E. Stoller, D.J. Bacon, A.F. Calder, J. Nucl. Mater. 223 (1995) 245.
[53] S.J. Zinkle, B.N. Singh, J. Nucl. Mater. 199 (1993) 173.

[54] K. Nordlund, L. Wei, Y. Zhong, R.S. Averback, Phys. Rev. B (Rapid Comm.) 57 (1998) 13965;
K. Nordlund, R.S. Averback, Phys. Rev. B 59 (1999) 20.
[55] D.A. Terentyev, L. Malerba, P. Olsson, M. Hou, in: A.I. Melker (Ed.), Proceedings of the 7th International Workshop on Nondestructive Testing and Computer Simulations in Science and Engineering, SPIE Proceedings, vol. 5400, The Society of Photo-Optical Instrumentation Engineers, 2004, ISBN 0-8194-5323-4.
[56] E.M. Lopasso, M. Caro, A. Caro, P.E.A. Turchi, Phys. Rev. B 68 (2003) 214205.
[57] C. Lagerstedt, D. Terentyev, P. Olsson, J. Wallenius, L. Malerba, in preparation.